AD-A075 816 AEROSPACE CORP EL SEGUNDO CA VEHICLE ENGINEERING DIV F/G 20/1
THE GENERATION OF A TOLLMIEN-SCHLICHTING WAVE BY A SOUND WAVE,(U)
AUG 79 J W MURDOCK N00014-78-C-0491
UNCLASSIFIED ATR-79(7775)-1 NL

| OF |
AD
A075816

END
DATE
FILMED
11-79
DDC

AEROSPACE REPORT NO.
ATR-79(7775)-1

The Generation of a Tollmien-Schlichting Wave by a Sound Wave

Prepared by

John W. Murdock
Vehicle Engineering Division

31 August 1979

Engineering Group
THE AEROSPACE CORPORATION
El Segundo, Calif. 90245

THE AEROSPACE CORPORATION

Aerospace Report No.
ATR-79(7775)-1

THE GENERATION OF A TOLLMIEN-SCHLICHTING WAVE BY A SOUND WAVE

Prepared by

John W. Murdock
Vehicle Engineering Division

31 August 1979

N0014-78-C-0491

Engineering Group
THE AEROSPACE CORPORATION
El Segundo, Calif. 90245

Report No.
ATR-79(7775)-1

THE GENERATION OF A TOLLMIEN-SCHLICHTING WAVE BY A SOUND WAVE

Approved

T. D. Taylor, Director
Fluid Dynamics Department
Aero Engineering Subdivision
Vehicle Engineering Division

ACKNOWLEDGMENTS

I would like to thank my colleagues for discussing this work with me and making suggestions for improvement. Drs. T. D. Taylor, J. Laufer and R. B. Myers were particularly helpful.

This work was sponsored by the Advanced Research Projects Agency under Office of Naval Research, Contract N0014-78-C-0491.

CONTENTS

FIGURES

Summary

A spectral numerical method is used to study the two-dimensional unsteady flow over a flat plate in the presence of a plane sound wave propagating parallel to the flow. For $s = \omega x/U_\infty > 0(1)$, no observable interaction or energy interchange between the sound wave and the Tollmien-Schlichting wave is present. In the region $s \leq 0(1)$, near the leading edge, an interaction occurs; the magnitude of this interaction is computed. A plane sound wave with dimensionless frequency $\omega\nu/U_\infty^2 = 56 \times 10^{-6}$ generates a Tollmien-Schlichting wave of the same frequency and an amplitude at the first neutral point 10^{-4} times the sound-wave amplitude. Computations at a second, lower frequency result in a lower neutral point amplitude. The response of the boundary layer to large unsteady disturbances is discussed and compared with published behavior based on the boundary layer equations. Solutions of the Orr-Sommerfeld equation are examined and found to have a different character for $s \lesssim 0(1)$ consistent with the more complete equations.

I. Introduction

The present work numerically investigates the flow over a flat plate in the presence of a plane sound wave propagating parallel to the free-stream flow. It is postulated that the sound wave generates Tollmien-Schlichting waves which, in turn, may lead to transition. Although the investigation considers only small amplitude sound waves, the numerical methods used are not restricted to this case.

An experimental study of the generation of Tollmien-Schlichting waves by sound waves has been made by Shapiro [1]. His data indicate that a Tollmien-Schlichting wave is generated with the same frequency as, and with a much smaller wave length than, the sound wave. Thomas and Lekoudis [2] compare Shapiro's data with a simple model in which the flow field is a sum of a Tollmien-Schlichting wave and a sound wave. This model is in fair agreement with Shapiro [1]; thus, they conclude that there is no interaction between the waves in the range of the data, and that the interaction which produced the Tollmien-Schlichting wave occurs near the leading edge.

The work on unsteady boundary-layer theory is relevant to the present work, even though the boundary-layer equations cannot predict the presence of Tollmien-Schlichting waves. Early work on unsteady boundary-layer theory was done by Moore [3] and Ostrach [4]. Illingworth [5] has addressed the problem of the interaction of a weak

sound wave with a compressible, heat-conducting boundary layer. He generates two series solutions for the perturbation to the Blasius flow. One expansion is valid for small dimensionless frequency, $s = \omega x/U_\infty$, and the other for large s. Lam and Rott [6] consider a general incompressible boundary layer with a small unsteady disturbance at the edge. They give special attention to the joining of the small s and large s solutions. Ackerberg and Phillips [7] consider incompressible flat-plate flow with small fluctuations in the free-stream velocity. Both investigations conclude that the downstream (large s) solution is approached asymptotically through damped eigenfunctions. Ackerberg and Phillips present numerical results to support this conclusion.

II. Physical and Mathematical Problem Description

The problem of interest is the interaction of a plane sound wave with a Blasius boundary layer in incompressible flow. Thus, the sound speed and wave length approach infinity and the wave number goes to zero. Following Illingworth [5], the dimensionless free-stream velocity is given by

$$u = 1 + \epsilon \cos\omega t \tag{1}$$

where ϵ is typically 10^{-3} in the results reported herein; ω and t are, respectively, the (temporal) frequency of the sound wave and time.

Going to the incompressible limit allows a previously developed computer code [8] to be applied with modifications only to the boundary conditions. Since a detailed description of the formulation, the assumptions, and the numerics has been reported, only a brief summary will be given here.

The equations are solved in dimensionless parabolic coordinates, ξ and η, which are related to the dimensional Cartesian coordinates, x and y, as follows:

$$x + iy = x_1 \left[\xi + i\eta \left(2R_{x_1} \right)^{-1/2} \right]^2 \tag{2}$$

where x_1 is a typical distance from the leading edge, and R_{x_1} is the Reynolds number based on the mean freestream velocity and x_1. The time is made dimensionless with the mean freestream velocity and with x_1

$$\tau = tU_\infty/x_1. \tag{3}$$

The dimensionless stream function and vorticity are defined in terms of the dimensional quantities ψ and ζ.

$$\psi = (2\nu U_\infty x_1)^{1/2} \xi f = (2\nu U_\infty x_1)^{1/2} g \tag{4}$$

$$\zeta = U_\infty [U_\infty/(2\nu x_1)]^{1/2} \Omega/\xi \tag{5}$$

where ν is the kinematic viscosity. The dependent variable f is the usual Blasius stream function.

The equations solved are the parabolized vorticity equations [8].

$$2\xi\Omega_\tau = \Omega_{\eta\eta}/\xi + g_\xi\Omega_\eta/\xi - g_\eta(\Omega/\xi)_\xi + \left[g_{\eta\eta}\Big/\left(2\xi^2 R_{x_1}\right)\right]_{\xi\xi} \tag{6}$$

$$\xi\Omega = g_{\eta\eta} + g_{\xi\xi}\Big/\left(2R_{x_1}\right). \tag{7}$$

The equation set is solved in the space

$$1 \le \xi \le \left(R_{x_2}/R_{x_1}\right)^{1/2} \tag{8}$$

$$0 \le \eta \le \infty \tag{9}$$

$$0 \le \tau \tag{10}$$

The equations are first order in time and are integrated from a Blasius initial condition at $\tau = 0$

$$g = \xi f = \xi f_{\text{Blasius}} \tag{11}$$

The four boundary conditions in the η-dimension are

$$g = g_\eta = 0; \qquad \eta = 0 \tag{12}$$

$$\left.\begin{aligned} g_\eta/\xi &= f_\eta = 1 + \epsilon\cos\omega t \\ g/\xi &= f = \eta - \beta + \epsilon(\eta-\gamma)\cos\omega t \end{aligned}\right\} \quad \eta \to \infty \tag{13}$$

where β is a constant characteristic of the displacement thickness and γ is either $\beta/2$ or zero in order to be consistent with the boundary conditions at R_{x_1}, discussed subsequently.

Posing the problem on a finite Reynolds number range [re Eq. (8)] has the advantage that the difficult to treat vortical singularity at the leading edge of the plate is avoided. On the other hand, it introduces a requirement for boundary conditions to be imposed at R_{x_1}. The boundary conditions are obtained from the unsteady boundary-layer solutions [5-7]. The small $s = \omega x/U_\infty$ solution for the x-component of the velocity is

$$u = f'_B + \epsilon\cos\omega t\left[f'_B + \eta f''_B/2 + O(s)\right] \tag{14}$$

where f_B is the Blasius solution. The solution for large s is

$$u = f'_B + \epsilon\left[\cos\omega t - \exp(-ky)\cos(\omega t - ky) + O(s^{-1/2})\right] \tag{15}$$

where

$$k = (\omega/2\nu)^{1/2} \tag{16}$$

The mixture of independent variables in Eq. (15) is used to emphasize the physics of that equation. Equation (14) shows that near the leading edge the unsteady velocity profile is in phase with the free

stream, and the thickness grows at the same rate as the Blasius boundary-layer thickness. For $s > 1$, Eq. (15) shows that the unsteady shear layer no longer grows with x, and that there is a phase shift across the Stokes-type layer. For large s, in the words of Ackerberg and Phillips [7], there is a "double boundary layer" with the Stokes layer being thinner than, and embedded in, the Blasius boundary layer.

The upstream boundary conditions obtained from Eqs. (14) and (15) are

$$g = g_{\xi} = f_B + \epsilon \cos\omega t \left(f_B + f'_B \right) \Big/ 2 \tag{17}$$

Equations (17) follow from Eq. (14); the conditions obtained from Eq. (15) are

$$\begin{aligned} g &= f_B + \epsilon \Big[\eta \cos\omega t + \Big\{ \exp[-K\eta][\cos(\omega t - K\eta) + \sin(\omega t - K\eta)] \\ &\quad - \cos\omega t - \sin\omega t \Big\} \Big/ 2K \Big] \\ g_{\xi} &= f_B + \epsilon\eta[\cos\omega t - \exp(-K\eta)\cos(\omega t - K\eta)] \end{aligned} \tag{18}$$

where K is a dimensionless k

$$K = kx_1 \left(R_{x_1} \Big/ 2 \right)^{-1/2} \tag{19}$$

The parabolized system of equations is third order in ξ and requires a downstream boundary condition. The present numerical results confirm previous experience [8] in which the condition

$$g_{\xi\xi\xi} = 0 \tag{20}$$

produced a small disturbance at the downstream boundary.

The equations are solved using a spectral method in space; a Chebyshev polynomial expansion is used in each dimension. The solution is updated in time with an explicit finite difference method.

III. Continuous Wave-Wave Interaction

Two possible mechanisms for feeding energy into a Tollmien-Schlichting wave from a sound wave are investigated herein. One possibility is the existence of a continuous flow of energy into the Tollmien-Schlichting wave along the whole boundary layer. The other possibility is that the sound wave interacts with the boundary layer only in localized regions, and then the Tollmien-Schlichting wave propagates independently of the sound wave. In this section, the former possibility is investigated.

The study of the wave-wave interaction is complicated by the fact that the computer code generates solutions for a finite region on the plate. Thus, any solution obtained is dependent upon the assumed upstream boundary conditions. Furthermore, unless the upstream boundary conditions are specifically chosen to be orthogonal to the primary eigensolution of the Orr-Sommerfeld equation, a finite Tollmien-Schlichting wave will be generated by the conditions. In

this section, the objective is to investigate the possibility of a continuous interaction. This continuous interaction, if it exists, will be most easily found if the Tollmien-Schlichting wave generated by the upstream boundary condition is minimized. As will be shown subsequently, Eqs. (18) generate a very small Tollmien-Schlichting wave. The effect of the boundary condition on the solution is also clarified by moving the position of the boundary and by running computations in the Reynolds number range in which the boundary-generated wave decays.

Before the solutions are examined, some trigonometric identities will be presented to aid in their interpretation. If at some station in the boundary layer the sound wave generates a time periodic disturbance of amplitude A and the Tollmien-Schlichting wave generates a disturbance of amplitude B and real wave number α, then the total disturbance (at frequency ω) is

$$u = A\cos\omega t + B\cos(\alpha x - \omega t) \tag{21}$$

where A and B may be functions of y and slowly varying functions of x, and the origin of x is assumed to be such that the phase angle is zero. The Fourier amplitude of the disturbance at frequency ω is

$$C = (A^2 + B^2 + 2AB\cos\alpha x)^{1/2} \tag{22}$$

When $A \gg B$, Eq. (22) may be expanded to give

$$C = A + B\cos\alpha x + O(B^2). \tag{23}$$

Equation (21) assumes that A and B are independent or weakly dependent parameters. Equation (23) shows that, in this case, the Fourier amplitude of the total disturbance will oscillate spatially with a wave length equal to the Tollmien-Schlichting wave length, that the magnitude of the spatial mean is associated with the sound wave, and that the magnitude of the envelope about the mean is associated with the Tollmien-Schlichting wave. The experimental data of Shapiro [1] are consistent with this picture in that he found the Fourier amplitude to oscillate spatially with the Tollmien-Schlichting wave length.

The first few figures show the results of a numerical calculation in the range $1.2 \times 10^5 \leq R_x \leq 3.8 \times 10^5$. The dimensionless frequency is that of Shapiro, $\omega\nu/U_\infty^2 = 5.6 \times 10^{-5}$. The large s boundary layer equations are used to generate the upstream boundary conditions [Eqs. (18)] imposed at $R_x = 1.2 \times 10^5$ or $s = 6.72$. The numerical solutions are obtained by running the calculations until the solution is time periodic; this solution can then be studied by Fourier transforming in time.

In Fig. 1, the Fourier amplitude of u at frequency ω is plotted versus Reynolds number for y = constant ($R_y = yU_\infty/\nu \approx 196$). This value of y corresponds to $\eta = 0.4$ at $R_x = 1.2 \times 10^5$. For the computation shown, the value of ϵ was 0.001 [re Eq. (1)]. (Numerical evidence obtained by repeating selected computations with ϵ halved verified that solutions with this value of ϵ are linear in ϵ.) The solution has the features of the sum of a Stokes layer solution and a Tollmien-Schlichting wave solution. The mean curve in Fig. 1 is very nearly

ant, corresponding to the fact that the high Reynolds number
ady boundary-layer solution (Stokes layer) is a function only
The solution oscillates about the mean with a wave length equal
Tollmien-Schlichting wave length (shown as λ in Fig. 1).

der to confirm the presence of a Tollmien-Schlichting wave, the
itude of the envelope of several curves similar to Fig. 1 was
ned and plotted versus η in Fig. 2 at $R_x = 2.8 \times 10^5$. The points
tained are compared with a scaled solution to the Orr-Sommerfeld
ion at the same Reynolds number, and the agreement is excellent.
e 2 shows that a Tollmien-Schlichting wave is present, and that
nvelope of curves such as Fig. 1 characterize the magnitude of
ave.

ave envelope points are shown for values of η greater than about
because at the larger values of η the solution curves appear to be
lated with two spatial wave lengths rather than just one, making
xtraction of the required information very difficult. Figure 3
s a plot of such a solution curve at a location twelve times further
the wall than the solution in Fig. 1. The value of y in Fig. 3
sponds to a value of η of 4.8 at $R_x = 1.2 \times 10^5$ and, for compari-
with Fig. 2, $\eta \approx 3.14$ at $R_x = 2.8 \times 10^5$. The spatial modulation
Tollmien-Schlichting wave length is still in evidence, but a
lation with a wave length about three times as long is also present.
ems likely that the longer wavelength modulation indicates the
nce of disturbances described by the continuous spectrum of the
Sommerfeld equation [9]. Continuous spectrum solutions are very
l in the boundary layer compared to their value further from the
This is consistent with the fact that the higher wave length
lation is not seen on Fig. 1. Furthermore, the dimensionless
speed of the continuous spectrum modes is very close to unity,
ared to a Tollmien-Schlichting wave speed, in the present case,
out 0.32. Thus, the factor of three difference in wave speed is
stent with the factor of three difference in modulation wave length
g. 3.

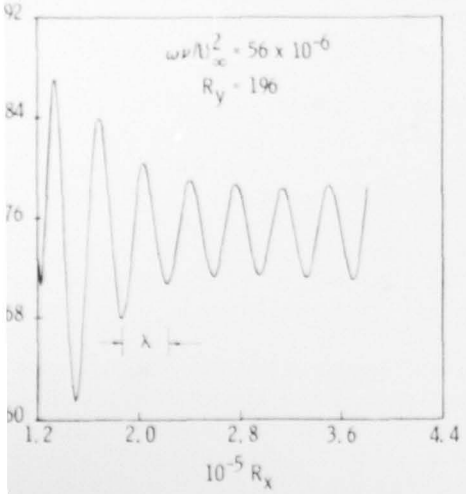

. 1. Fourier amplitude of u
onstant y

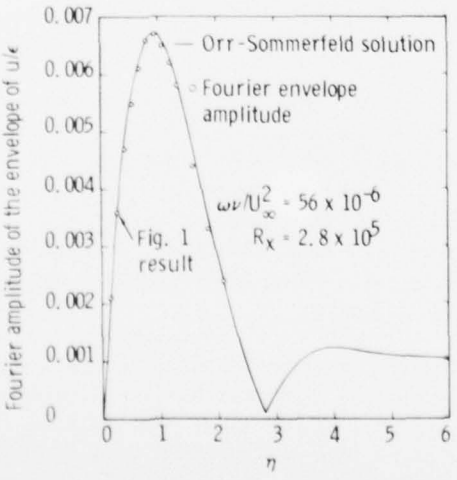

Fig. 2. Variation of envelope of u across the boundary layer

The main interest here is the generation of Tollmien-Schlichting waves; thus, most of the remainder of the plots will be at a y-location very near the wall ($R_y = 196$). In all cases, this was sufficient to suppress the continuous spectrum disturbances which were evident further out in the boundary layer. Any other discrete eigenmodes present decay very rapidly.

Figure 4 shows the variation of the total Fourier amplitude of u versus y at the upstream boundary, and in the interior of computation domain. The upstream boundary condition has been imposed at $R_x = 1.2 \times 10^5$, so the left curve in Fig. 4 is just the Fourier amplitude of Eq. (15). This figure demonstrates that the high Reynolds number boundary layer solution is an excellent approximation to the solution of the more complete equations. Any deviation of the right-hand curve of Fig. 4 from the (left-hand) boundary-layer solution because of the presence of the Tollmien-Schlichting or continuous spectrum waves is imperceptible on the scale of Fig. 4.

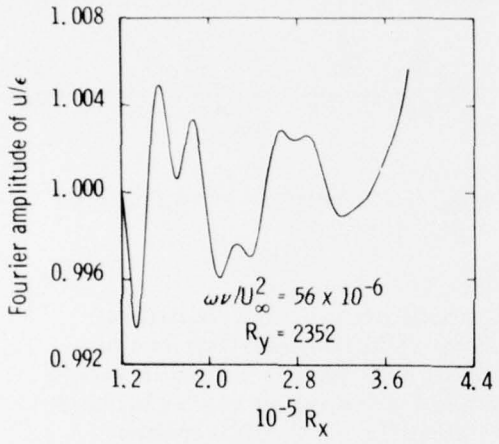

Fig. 3. Fourier amplitude at constant y

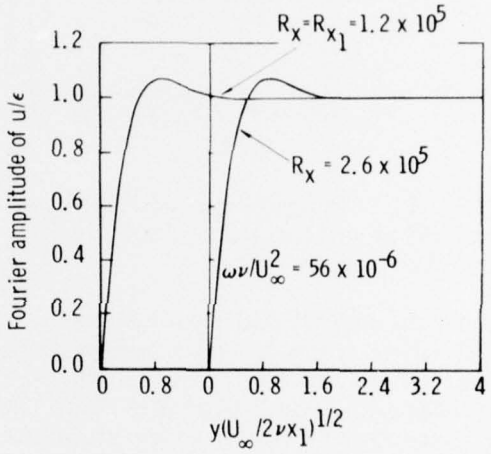

Fig. 4. Fourier amplitude of u versus y

Figures 1 through 4 demonstrate that a Tollmien-Schlichting wave is present. The main interest of this paper is the source of this wave. The spatial amplitude variation of the Tollmien-Schlichting wave in the presence of the sound wave is compared with the variation of a pure Tollmien-Schlichting wave with no sound wave present. If the curves have the same behavior, then the Tollmien-Schlichting wave propagates independently of the sound wave; if the envelope curve grows relative to the pure wave amplitude, then energy is fed into the Tollmien-Schlichting wave continuously by the sound wave. The circles in Fig. 5 are obtained from the extrema of Fig. 1; the curve is a scaled linear Tollmien-Schlichting wave solution with no sound wave present. With the exception of the first point, they are in good agreement. At the first point, other decaying eigenmodes are non-negligible. It is concluded that the Tollmien-Schlichting wave in the numerical computation is generated by the boundary condition at the upstream boundary and subsequently propagates independently of the sound wave. As noted previously, Thomas and Lekoudis [2] have concluded from Shapiro's data that the two waves are independent.

Figure 6 further demonstrates that the Tollmien-Schlichting wave amplitude in the present computations is controlled by the upstream boundary conditions. The upstream boundary has been moved from 1.2×10^5 in Fig. 1 to 1.1×10^5 in Fig. 6; all other parameters are unchanged. The phase and amplitude are significantly affected by the change in location of the upstream boundary, rather than being independent of the boundary condition as would be the case if interaction with the freestream sound wave dominated.

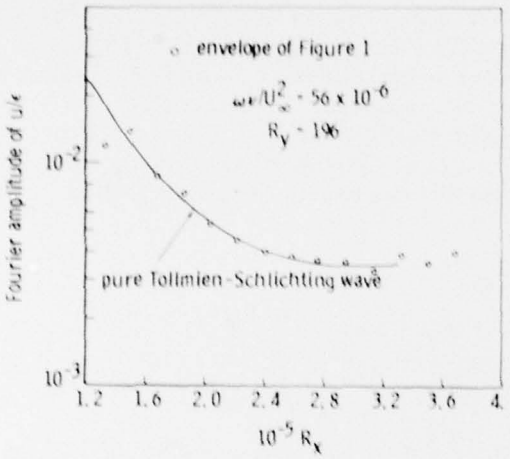

Fig. 5. Comparison of envelope behavior with a pure Tollmien-Schlichting wave

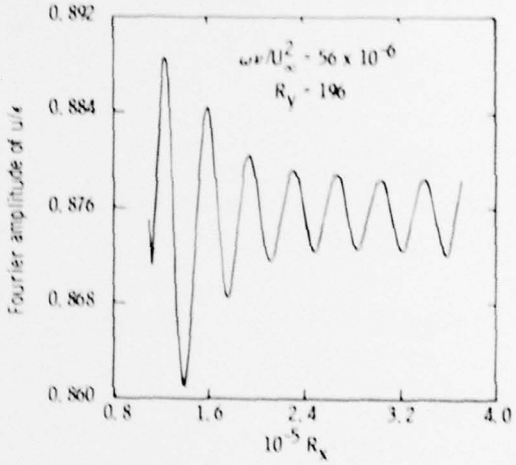

Fig. 6. Fourier amplitude of u at constant y

The main result of this section is that a small amplitude Tollmien-Schlichting wave may be added to the Stokes solution and that these waves or solutions do not interact, in the high Reynolds number range considered. The Tollmien-Schlichting waves present in the solutions discussed were found to be generated artificially by the upstream boundary condition.

IV. Localized Wave-Wave Interaction

In the previous section, it was concluded that the interaction between a sound wave and a Tollmien-Schlichting wave does not occur over the entire boundary layer but, if it occurs, the interaction is confined to a localized region. The purpose of this section is to determine where energy is fed into the Tollmien-Schlichting wave and to compute the amplitude of this wave.

Some of the major results of unsteady boundary-layer theory will be summarized in order to place the numerical results in perspective. In the boundary layer case, there are two distinct solution regions on the plate. At low Reynolds number, the unsteady layer grows at the same rate as the Blasius boundary layer; at high Reynolds number, the unsteady layer is controlled by the frequency and is thinner than the Blasius layer. There is little doubt that the more complete equations considered herein have solutions with essentially the same behavior as Fig. 4 has demonstrated. The authors of Refs. 6 and 7 were concerned with explaining how the parabolic boundary-layer equations could always have the same large Reynolds number solution, independent of

any disturbances which might exist upstream. They conclude that the downstream solution is approached via damped eigenfunctions; disturbances inconsistent with the downstream solution generate asymptotic eigensolutions which decay exponentially. Numerical solutions to the parabolized vorticity equations will be shown to be similar. Even with large disturbances (introduced via the upstream boundary conditions), the solution at large Reynolds number approaches the expected downstream solution via eigenfunctions. There is one major difference, however; the asymptotic eigenfunction (not present in the boundary-layer approximation) associated with the Tollmien-Schlichting wave is not necessarily damped. The following picture will be developed. Under normal flow conditions (no localized disturbance), the magnitude of the various eigenfunctions including the Tollmien-Schlichting wave amplitude in the case of the more complete equations is set by the end of the region in which the unsteady boundary layer changes from a growing to a constant-thickness layer. If disturbances are introduced at some point downstream of this region, then the magnitude of the eigenfunctions is set immediately downstream of the disturbance.

All the numerical results reported in this section use Eq. (17) as the upstream boundary condition on the computation. Physically, the use of this boundary condition is only justified for s small compared to unity. Computations were actually performed in which the upstream value of s was varied from 6.16 to 0.392. Using Eq. (17) at high Reynolds number is a way of inputting a large disturbance at high Reynolds number. Results from these computations will be used to demonstrate that the solution does relax to the expected high Reynolds number behavior.

Numerical instabilities were encountered when the first attempts were made at running computations with small upstream Reynolds number. It was ultimately found that with 33 Chebyshev modes in the streamwise direction, the requirement for numerical stability is

$$R_{x_2} / R_{x_1} < 3.9 \qquad (24)$$

This is a severe restriction, because the physical length of the computation varies linearly with the upstream Reynolds number R_{x_1}, and the interest is in small values of R_{x_1}. At larger values of R_{x_1}, the length of the computation is restricted to about eight Tollmien-Schlichting wavelengths with the 33 modes. Because of the restriction, no computations were made with a value of s at the upstream boundary smaller than 0.392.

Consider first a calculation which is identical to Fig. 5, except that the upstream boundary condition has been changed from Eq. (15) to Eq. (14). The boundary condition is physically correct for small s, so it is here interpreted as a solution with a large periodic disturbance input at $s = 6.16$, $R_x = 1.1 \times 10^5$. A plot of the Fourier amplitude of u at constant y analogous to Fig. 6 is shown in Fig. 7. The two curves are qualitatively very similar; after a finite region at the left-hand end in which continuous and higher discrete modes decay, both are modulated with the same Tollmien-Schlichting wavelength and have the same envelope decay rate and mean value. The major difference is that the Tollmien-Schlichting wave (the envelope) amplitude

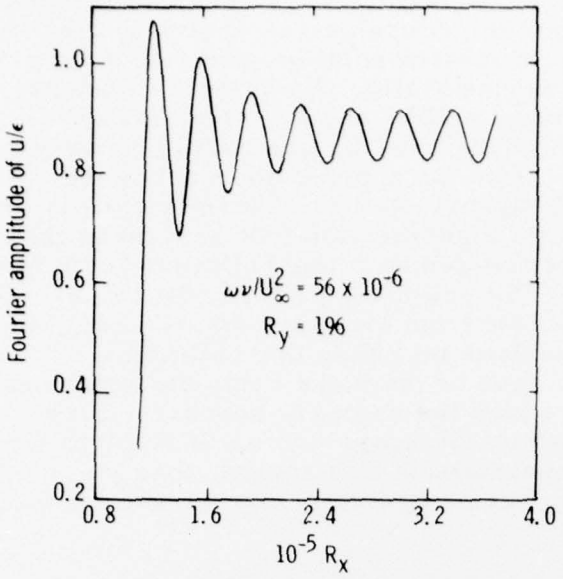

Fig. 7. Fourier amplitude of u at constant y

is about a factor of 16 larger in Fig. 7 than in Fig. 6. It is also interesting to look at the profile of the Fourier amplitude of u versus y and see how it changes as a function of Reynolds number. Such curves are shown in Figs. 8 and 9. The curve for Reynolds number 1.1×10^5 in Fig. 8 is the upstream boundary condition or, alternatively, the unsteady disturbance. The characteristic thickness of this disturbance is much greater than the normal Stokes layer which would exist at that frequency and Reynolds number. Figures 8 and 9 show that the boundary layer has adjusted to a solution similar to those shown in Fig. 4 by Reynolds number 2×10^5. Downstream of $R_x = 2 \times 10^5$ the characteristic shape shown in Fig. 4 persists, subject to some small modification near the peak of the Tollmien-Schlichting wave ($\eta \approx 1$). Figures 6-8 show that the present solutions have the same behavior as the boundary layer solutions--they approach the same high Reynolds number solution via their respective eigenfunctions.

It was not possible to carry out numerical computations with the upstream boundary at an arbitrarily small Reynolds number. Thus, computations have been carried out with several upstream boundary locations, and the results are extrapolated to smaller values.

In Fig. 10, the amplitude of several Tollmien-Schlichting waves generated by imposing the boundary condition (14) at different locations is plotted versus Reynolds number. These curves are obtained from the respective envelope curves, the uppermost curve being obtained from Fig. 7. There is no numerical evidence that the amplitude of the Tollmien-Schlichting waves is affected by the presence of the sound wave subsequent to their generation at the upstream boundary. This may be verified by noting that to within numerical accuracy the curves in Fig. 10 are each a constant multiple of any other curve. This is the expected behavior of a linear Tollmien-Schlichting wave; the rate of decay-growth is independent of amplitude. In those cases in which the computation did not extend to the neutral (minimum) point, $R_x \approx 3 \times 10^5$, the curves have been extrapolated using the appropriate

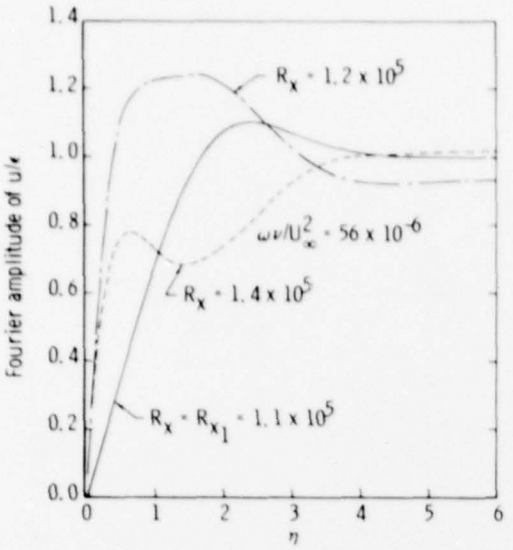

Fig. 8. Variation of Fourier amplitude across boundary layer

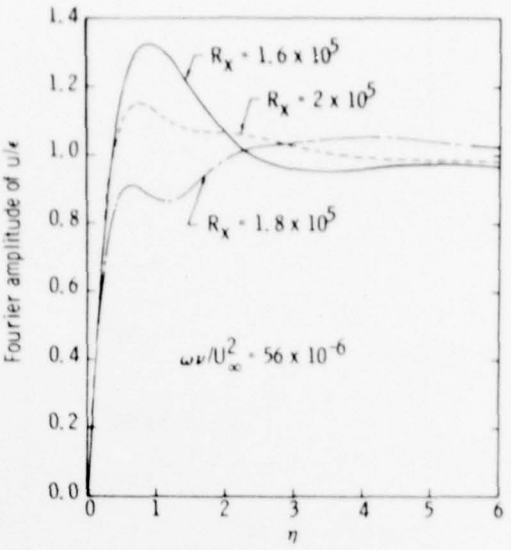

Fig. 9. Variation of Fourier amplitude across boundary layer

constant and are shown on the figure as dashed lines. Each of the curves in Fig. 10 was obtained from a single numerical computation except for the lower curve with $R_{x_1} = 10^4$. This curve was obtained with three overlapping computations with Reynolds number ranges $10^4 \leq R_x \leq 3.9 \times 10^4$, $29487 \leq R_x \leq 1.15 \times 10^5$, and $82626 \leq R_x \leq 3.2 \times 10^5$. Restarting the calculation introduces a substantial amount of noise into the computation. Because of this noise problem and the limit in Eq. (24), no computations were attempted with R_{x_1} less than 7×10^3. Increasing the number of modes in the ξ-direction would allow R_{x_1} to be reduced further but was rejected because of computer cost considerations.

The numerical results presented are consistent with the boundary layer model studied in Refs. 6 and 7. In the boundary layer case, the large Reynolds number solution is approached via asymptotic, decaying eigenfunctions. The amplitude of these eigenfunctions is determined uniquely by the upstream boundary condition, and the sound wave does not feed further energy into these eigenmodes at downstream locations. In the present case, the eigenmodes of interest are those associated with the Orr-Sommerfeld equation and are different from the modes of the boundary layer equations. The numerics have been concentrated on the Tollmien-Schlichting mode. Analogous to the boundary-layer case, the amplitude of this mode is set by the upstream boundary condition, and no further energy is found to be fed into it at downstream stations. In the limiting case wherein the boundary condition is imposed arbitrarily close to the leading edge, the eigenmodes in both cases are still uniquely determined. However, these eigenmodes are asymptotic solutions valid only for $s > 1$. (It is shown in the next section that the solutions to the Orr-Sommerfeld equation only make physical sense for $s > 1$.) In this context, the region $0 \leq s \leq 0(1)$ is the region in which the boundary layer and the sound wave interact. The output of this region is a set of asymptotic

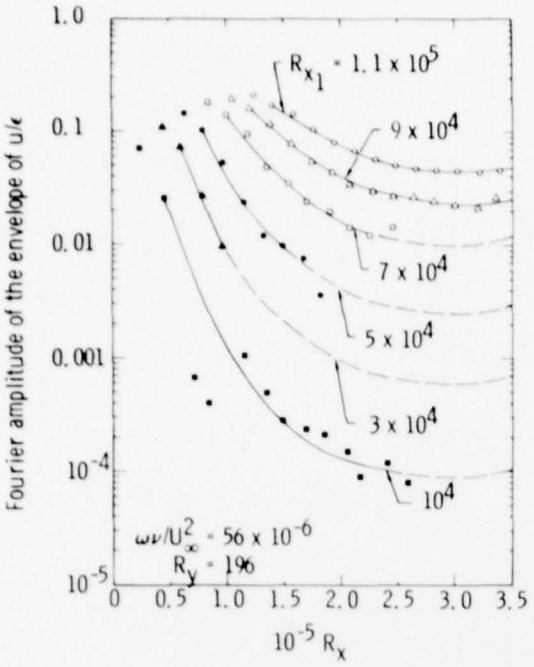

Fig. 10. Fourier envelope of u versus Reynolds number

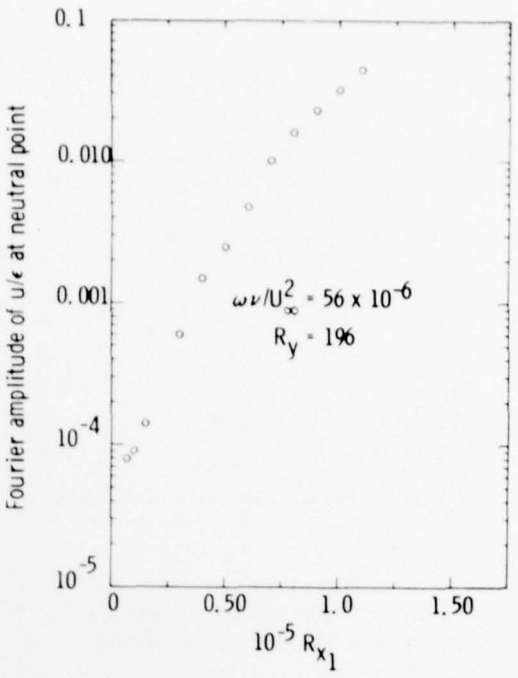

Fig. 11. Amplitude at neutral point versus R_{x_1}

linear solutions which are physically and mathematically independent. Among these independent solutions are the Tollmien-Schlichting wave and the Stokes layer solution.

The neutral (minimum) amplitude, obtained from Fig. 10 and similar curves, is plotted in Fig. 11 as a function of the upstream boundary location. This includes three points obtained from computations with $s < 1$ at R_{x_1}. The neutral value for $R_{x_1} = 0$ is the amplitude of a Tollmien-Schlichting wave generated by a sound wave with dimensionless frequency 56×10^{-6} at $R_y = 196$. By extrapolation of Fig. 11, this neutral amplitude is estimated to be $5.5 \pm 1.5 \times 10^{-5}$. The neutral point amplitude of the Tollmien-Schlichting wave at $R_y = 196$ (Fig. 2) is about half the peak amplitude. Thus, the peak amplitude of the sound-generated Tollmien-Schlichting wave is $1.0 \pm 0.3 \times 10^{-4}$ times the sound wave amplitude.

The frequency of the sound wave and the Tollmien-Schlichting wave in the computations described up to this point is $\omega\nu/U_\infty^2 = 56 \times 10^{-6}$. This value was chosen to coincide with Shapiro's [1] experimental frequency. There is substantial disagreement between this experimental work and the present numerical computations. Based upon Shapiro's Figure 28, the Tollmien-Schlichting wave amplitude at the neutral point is about 0.4 times the sound wave amplitude, while the present computations suggest a value of 10^{-4}. There are two possible reasons for this discrepancy. The data were obtained on an elliptical-nosed model with a significant pressure gradient up to Reynolds numbers greater than 10^5. Thus, the data and the computations are not strictly comparable. Another possibility is that the sound wave in the

experiments was not exactly a plane wave and thus effectively generated local disturbances. The numerical results of this section suggest that a localized disturbance can generate a larger Tollmien-Schlichting wave than a plane wave disturbance.

A brief investigation has been made with a smaller frequency of the disturbing sound wave. Figure 12 is a plot identical to Fig. 10, except that the dimensionless frequency has been halved to 28×10^{-6}. This frequency is approximately the frequency at which the total growth of the Tollmien-Schlichting wave in the unstable region is e^9, as shown for example by Jaffe, Okamura and Smith [10]. Although only two computations have been made at this frequency, the behavior is similar to that at the higher frequency. The neutral point amplitudes from Fig. 12 are shown in Fig. 13. A linear extrapolation of these results to zero upstream Reynolds number gives a wave amplitude of 3×10^{-5} times the sound wave amplitude. Note, however, that the results in Fig. 11 suggest that the linear extrapolation may be a factor of two or three too high. Again, taking into account the fact that the plotted results are not at the peak of the Tollmien-Schlichting wave, the linearly extrapolated result gives a peak wave amplitude at the first neutral point of 7×10^{-5} times the sound wave amplitude. Thus, it is concluded that halving the sound wave frequency decreases the peak Tollmien-Schlichting wave amplitude by 30 to 70 percent.

On a sharp, flat plate, a plane sound wave interacts with the boundary layer very near the leading edge and generates a Tollmien-Schichting wave which can first be identified as such downstream of the $s \leq 0(1)$ region. This wave propagates unaffected by the sound wave after it appears. Between $s = 0(1)$ and the neutral point, the wave decays

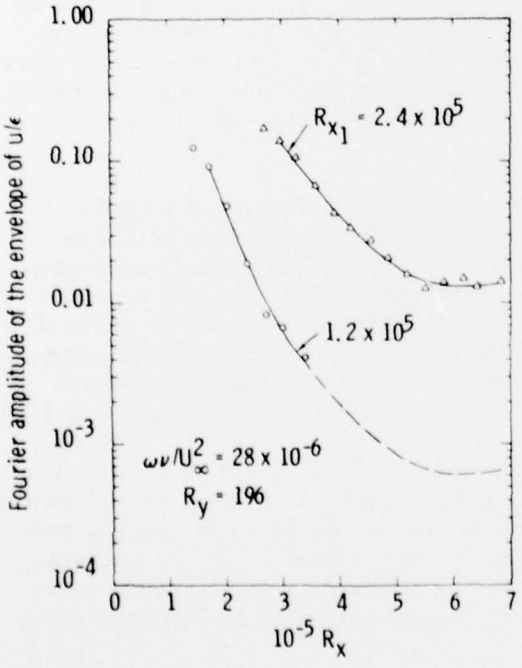

Fig. 12. Fourier amplitude of u versus Reynolds number

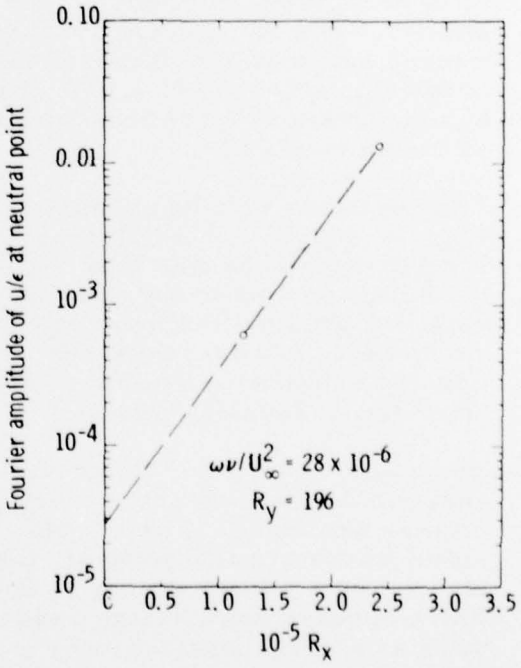

Fig. 13. Amplitude at neutral point versus R_{x_1}

substantially, to about 10^{-4} times the sound wave amplitude at the neutral point. This is small, but it should be noted that a total Tollmien-Schlichting wave growth of $e^9 \approx 10^4$ downstream of the neutral point is frequently used to empirically correlate transition. The results of this section also suggest that localized disturbances may generate larger amplitude Tollmien-Schlichting waves than the plane wave disturbance.

V. Solutions to the Orr-Sommerfeld Equation

In this section, the behavior of solutions to the Orr-Sommerfeld equation in the regions $s \leq 0(1)$ and $s > 0(1)$ are studied. These solutions provide further confirmation of the difference in the physics of unsteady boundary layers in the two regions.

The Orr-Sommerfeld equation (i.e., see Schlichting [11]) is obtained by linearizing the Navier-Stokes equations and then representing the disturbance in the form $\phi(y) \exp i(\alpha x - \omega t)$. The spatial eigenfunctions in which ω is real and α is complex are of interest here. It should be emphasized that the variation of α with x or R_x is implicitly assumed to be negligible, since the derivative with respect to x is taken as $i\alpha\phi \exp i(\alpha x - \omega t)$.

The primary spatial eigenvalue is plotted in Fig. 14 as a function of Reynolds number. The emphasis is on low Reynolds number, and the well-known unstable region is not computed. (The numerical method used is described in the Appendix of Ref. 9.) Above a Reynolds number of about 6.5×10^4, the real part of α has a slight negative slope corresponding to the small increase in Tollmien-Schlichting wave length with Reynolds number. Starting from the continuous spectrum at $R_x \approx 62.9$, $Re\alpha\nu/U_\infty$ grows, rapidly at first, from a value of about 0.535×10^{-4}. (The relationship between the discrete and continuous spectrum is discussed in Refs. 9 and 12.) The imaginary part of $\alpha\nu/U_\infty$ is about 232×10^{-4} at the continuous spectrum and decreases by two orders of magnitude with the higher Reynolds number behavior, as shown in Fig. 14.

The minimum wavelength associated with the maximum of $Re\alpha$ in Fig. 14 is $R_\lambda = 3.3 \times 10^4$; thus, below a Reynolds number of about 3×10^4, large changes in α occur in one wave length. The assumption ($\phi_x = i\alpha\phi$) leading to the Orr-Sommerfeld equation is violated, and a different physical model is required in this region. Thus, the physical entity which is approximately modeled by the Orr-Sommerfeld equation and known as a Tollmien-Schlichting wave can only exist above some finite Reynolds number; in the present case this is about 3×10^4.

The solutions of the Orr-Sommerfeld equation are consistent with the numerical solutions of the more complete equations in that two distinct regions are found. For $s > 0(1)$, where the Tollmien-Schlichting and sound waves are independent, the Orr-Sommerfeld model is satisfactory. For $s < 0(1)$, energy is fed into the Tollmien-Schlichting wave which appears downstream, and the Orr-Sommerfeld equation breaks down as a valid physical model.

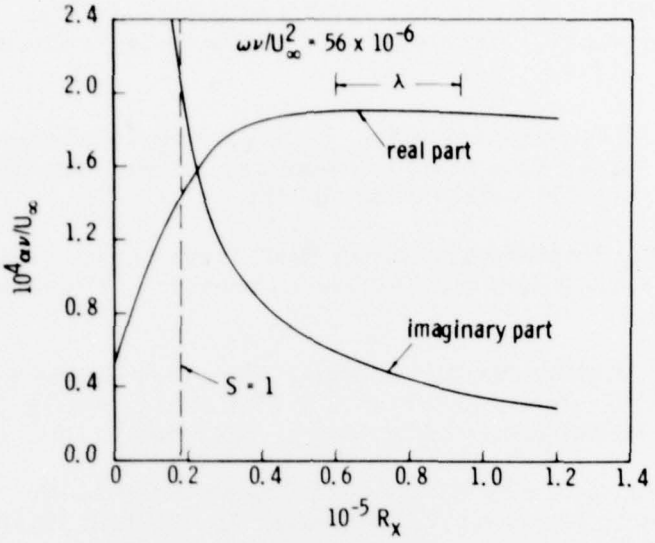

Fig. 14. Spatial eigenvalues of the Orr-Sommerfeld equation

VI. Concluding Remarks

The major results to emerge from this study are as follows. For nearly incompressible flow (sound wave length large compared to Tollmien-Schlichting wave length), plane sound waves feed energy into Tollmien-Schlichting waves only very near the leading edge; over most of the boundary layer the two waves are totally independent. Predictions have been made of the amplitude of a Tollmien-Schlichting wave generated by free-stream disturbances; the physical understanding achieved in this work will aid future studies of other types of free-stream disturbances. The response of the boundary layer to localized unsteady disturbances has been extensively studied. These results show that much larger Tollmien-Schlichting waves can be generated by local disturbances and, thus, should be more important in the ultimate transition process. Solutions of the Orr-Sommerfeld equation are found to change character near $s = 0(1)$; the solutions for $s < 0(1)$ suggest that Tollmien-Schlichting waves do not occur in this small region near the leading edge of the plate.

References

1. Shapiro, P.J.: The Influence of Sound upon Laminar Boundary Layer Instability, Report No. 83458-83560-1, Acoustics and Vibration Laboratory, Massachusetts Institute of Technology, Cambridge, Mass. (Sept. 1977).

2. Thomas, A.S.W. and Lekoudis, S.G.: Sound and Tollmien-Schlichting Waves in a Blasius Boundary Layer, The Physics of Fluids, 21, 11, 2112-2113 (Nov. 1978).

3. Moore, F.K.: Unsteady Laminar Boundary-Layer Flow, NACA TN 2471, Lewis Flight Propulsion Laboratory, Cleveland, Ohio (Sept. 1951).

4. Ostrach, S.: Compressible Laminar Boundary Layer and Heat Transfer for Unsteady Motions of a Flat Plate, NACA TN 3569, Lewis Flight Propulsion Laboratory, Cleveland, Ohio (Nov. 1955).

5. Illingworth, C.R.: The Effects of a Sound Wave on the Compressible Boundary Layer on a Flat Plate, J. of Fluid Mech., 3, 471-493 (1958).

6. Lam, S.H. and Rott, N.: Theory of Linearized Time-Dependent Boundary Layers, AFOSR TN-60-1100, Graduate School of Aeronautical Engineering, Cornell University, Ithaca, New York (July 1960).

7. Ackerberg, R.C. and Phillips, J.H.: The Unsteady Laminar Boundary Layer on a Semi-Infinite Flat Plate due to Small Fluctuations in the Magnitude of the Free-Stream Velocity, J. of Fluid Mech., 51, 1, 137-157 (1972).

8. Murdock, J.W.: A Numerical Study of Nonlinear Effects on Boundary Layer Stability, AIAA J., 15, 8, 1167-1173 (Aug. 1977).

9. Murdock, J.W. and Stewartson, K.: Spectra of the Orr-Sommerfeld Equation, The Physics of Fluids, 20, 9, 1404-1411 (Sept. 1977).

10. Jaffe, N.A., Okamura, T.T. and Smith, A.M.O.: Determination of Spatial Amplification Factors and Their Application to Predicting Transition, AIAA J., 8, 2, 301-308 (1970).

11. Schlichting, H.: Boundary Layer Theory, 4th ed., McGraw-Hill Book Co., Inc., New York, 383-386 (1960).

12. Mack, L.M.: A Numerical Study of the Temporal Eigenvalue Spectrum of the Blasius Boundary Layer, J. of Fluid Mech., 73, 3, 497-520 (1976).

difference in modulation wave length

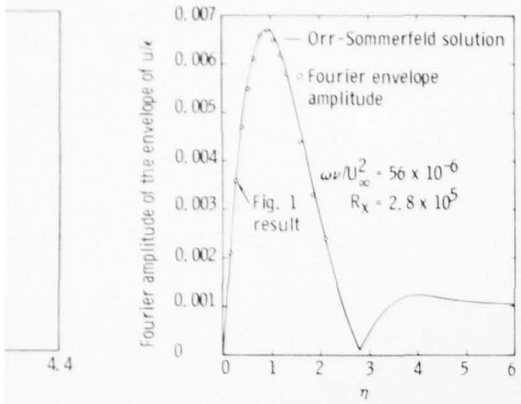

of u

Fig. 2. Variation of envelope of u across the boundary layer